# How Does Tidal Flow Affect Pattern Formation in Mussel Beds?

# How Does Tidal Flow Affect Pattern Formation in Mussel Beds?

Jonathan A. Sherratt, Julia J. Mackenzie


www.elsevier.com/locate/yjtbi

PII: S0022-5193(16)30161-8
DOI: http://dx.doi.org/10.1016/j.jtbi.2016.06.025
Reference: YJTBI8713

To appear in: *Journal of Theoretical Biology*

Received date: 8 March 2016
Revised date: 6 June 2016
Accepted date: 20 June 2016

Cite this article as: Jonathan A. Sherratt and Julia J. Mackenzie, How Does Tida Flow Affect Pattern Formation in Mussel Beds?, *Journal of Theoretical Biology* http://dx.doi.org/10.1016/j.jtbi.2016.06.025

# How Does Tidal Flow Affect Pattern Formation in Mussel Beds?

Jonathan A. Sherratt, Julia J. Mackenzie

Department of Mathematics and Maxwell Institute for Mathematical Sciences,
Heriot-Watt University, Edinburgh EH14 4AS, UK
E-mail: j.a.sherratt@hw.ac.uk, jjm33@hw.ac.uk

## Abstract

In the Wadden Sea, mussel beds self-organise into spatial patterns consisting of bands parallel to the shore. A leading explanation for this phenomenon is that mussel aggregation reduces losses from dislodgement and predation, because of the adherence of mussels to one another. Previous mathematical modelling has shown that this can lead to spatial patterning when it is coupled to the advection from the open sea of algae – the main food source for mussels in the Wadden Sea. A complicating factor in this process is that the advection of algae will actually oscillate with the tidal flow. This has been excluded from previous modelling studies, and the present paper concerns the implications of this oscillation for pattern formation. The authors initially consider piecewise constant ("square-tooth") oscillations in advection, which enables analytical investigation of the conditions for pattern formation. They then build on this to study the more realistic case of sinusoidal oscillations. Their analysis shows that future research on the details of pattern formation in mussel beds will require an in-depth understanding of how the tides affect long-range inhibition among mussels.

## Key words

mussel, pattern, Floquet, reaction-diffusion-advection,
periodic travelling wave, Wadden Sea

## Running Title

Tidal Flow and Patterns in Mussel Beds

## Acknowledgements

We thank Johan van de Koppel (NIOZ-Yerseke)
for helpful comments on the manuscript.

# 1 Introduction

Over the last few decades, aerial photographs and satellite images have revealed landscape-scale patterns in a wide variety of ecosystems. The best-documented case is vegetation patterns in semi-arid environments, for which there is an extensive literature of both empirical research (e.g. Deblauwe *et al*, 2011; Pelletier *et al*, 2012; Sheffer *et al*, 2012) and mathematical modelling (e.g. Stewart *et al*, 2014; Siteur *et al*, 2014; Zelnik *et al*, 2015; Sherratt, 2015). Other examples include patterns of ridges and hollows in peatlands (Eppinga *et al*, 2008, 2009), linear patterns of trees such as "ribbon forest" (Bekker *et al*, 2009) and "Shimagare" (Suzuki *et al*, 2012), and patterned mussel beds, which are the subject of this paper. The self-organised formation of mussel patches on rocky shores has been studied via both field work and modelling for more than 40 years (Levin & Paine, 1974; Paine & Levin, 1981; Wootton, 2001). More recently, pattern formation has been studied in soft-bottomed mussel beds – the essential difference here is that the mussels adhere only to one another, not to the underlying substrate. Labyrinthine patterns are common in these systems (e.g. Snover & Commito, 1998), and have been replicated in laboratory and modelling studies (van de Koppel *et al*, 2008; Commito *et al*, 2014). In 2005, van de Koppel *et al* published the first report of larger scale regular patterning in mussel beds, which are shown in aerial photographs of the Wadden Sea (Figure 1). This is the largest unbroken system of intertidal sand and mud flats in the world, and is a Unesco World Heritage site; it lies off the coast of the Netherlands, Germany and Denmark. The patterns consist of stripes of mussels running parallel to the shore, separated by stripes of bare sediment, with a wavelength of about 6 m.

As well as documenting the mussel bed patterns, the paper of van de Koppel *et al* (2005) also presents a mathematical model that aims to explain them. In the Wadden Sea, mussel beds are subject to disruption by predation, wave action, and ice scouring (Donker *et al*, 2015). The basis of van de Koppel *et al*'s (2005) model is that these effects are reduced at higher mussel densities. Empirical data shows that mussel density does increase in response to both greater wave exposure (Tam & Scrosati, 2014) and greater predation threat (Cote & Jelnikar, 1999; Naddafi *et al*, 2010). Conversely, increased

Figure 1: An aerial photograph of a banded patterned mussel bed in the Dutch Wadden Sea. Photograph courtesy of Jasper Donker and reproduced from Donker (2015), with permission.

densities have been shown to give greater resilience to disturbances (Bertness & Grosholz, 1985). This is because mussels attach to their neighbours via byssal threads, with more attachments forming when mussels are subject to perturbations (wa Kangeri *et al*, 2014). Note that the absence of substrate attachments in soft-bottomed beds means that other mussels or shell fragments provide the only available anchorage.

The model of van de Koppel *et al* (2005) is formulated in terms of mussel density $m(x,t)$ and algal concentration $a(x,t)$, where $t$ is time and $x$ is a spatial coordinate running away from the shore. Algae are the main food source for mussels in the Wadden Sea, and their availability is the limiting factor for mussel growth (Dolmer, 2000; Oie *et al*, 2002). They reside primarily in upper water layers, where their concentration is maintained by advection from the open sea in the incoming tide, but there is some transport to lower layers where they become susceptible to predation by mussels. van de

Koppel *et al*'s (2005) model represents these various processes via the equations

$$\partial a/\partial t = \overbrace{\alpha(1-a)}^{\substack{\text{transfer to/}\\ \text{from upper}\\ \text{water layers}}} - \overbrace{am}^{\substack{\text{consumption}\\ \text{by mussels}}} + \overbrace{\beta\,\partial a/\partial x}^{\substack{\text{advection}\\ \text{by tide}}} \tag{1a}$$

$$\partial m/\partial t = \underbrace{\delta am}_{\text{birth}} - \underbrace{\gamma\, m/(1+m)}_{\substack{\text{dislodgement}\\ \text{by waves}}} + \underbrace{\partial^2 m/\partial x^2}_{\substack{\text{random}\\ \text{movement}}}. \tag{1b}$$

which have been non-dimensionalised (see van de Koppel *et al* (2005) for details); $\alpha$, $\beta$, $\gamma$ and $\delta$ are positive parameters. Note that although mussels are often thought of as sessile organisms, they actually move both within and between clusters (Toomey *et al*, 2002; Nicastro *et al*, 2008), and this is represented in a simple way by the diffusion term in (1b). More realistic modelling of mussel movement is discussed in Liu *et al* (2014b).

The model (1) has been studied in a number of recent papers. Wang *et al* (2009) and Liu *et al* (2012) presented numerical bifurcation studies providing details of pattern existence, and Sherratt (2013) extended this to examine pattern stability. Ghazaryan & Manukian (2015) used geometric singular perturbation theory to study travelling wave solutions of the model – both patterns and fronts; the latter includes moving transitions between patterned and non-patterned regions. Cangelosi *et al* (2015) extended the model by replacing the advection term in the algae equation by diffusion. Their weakly nonlinear analysis provides a detailed account of patterns in this amended model, which they compared with experimental data.

The present paper concerns exclusively the van de Koppel model (1) based on the "reduced losses" hypothesis, but it is important to remark that alternative mechanisms have been proposed for mussel bed patterning. In particular Liu *et al* (2012, 2014a) have developed a mathematical model based on a "sediment accumulation" hypothesis, namely that more rapidly growing mussels deposit greater amounts of sediment beneath them, which raises them towards their food source (algae) and thus further promotes their growth.

The advection term in (1a) plays a central role in pattern formation: it creates a long-range inhibition between mussels that combines with the short-range activation arising from the density-dependent loss term in (1b) to generate patterns. Advection also plays an

important role in other types of landscape-scale patterning, including vegetation patterns. Labyrithine or spotted patterns of semi-arid vegetation occur on flat ground, but the propensity for patterning is increased on slopes, where one typically sees banded patterns running parallel to the contours (Deblauwe *et al*, 2008, 2011; Meron, 2012; Siteur *et al*, 2014). This is due to the downhill advection of rain water, which is the key resource in semi-arid ecosystems and therefore plays a role analogous to that of algae in mussel beds in the Wadden Sea.

The original presentation of the model (1) (van de Koppel *et al*, 2005) and the subsequent papers studying the model all use a unidirectional advection term, except for Cangelosi *et al* (2015) who replaced the advection term with diffusion. This is based on the assumption that the most important process in the supply of algae is their advection from the open sea on the incoming tide. However in reality algae are advected both towards the shore by the incoming tide, and away from it by the outgoing tide. In the present paper we will use a bidirectional advection term, and investigate the implications of this for pattern formation. Specifically, we will study the equations

$$\partial a/\partial t = \overbrace{\alpha(1-a)}^{\substack{\text{transfer to/}\\ \text{from upper}\\ \text{water layers}}} - \overbrace{am}^{\substack{\text{consumption}\\ \text{by mussels}}} + \overbrace{\beta\,\mathcal{B}(t)\partial a/\partial x}^{\substack{\text{advection}\\ \text{by tide}}} \tag{2a}$$

$$\partial m/\partial t = \underbrace{\delta am}_{\text{birth}} - \underbrace{\gamma\, m/(1+m)}_{\substack{\text{dislodgement}\\ \text{by waves}}} + \underbrace{\partial^2 m/\partial x^2}_{\substack{\text{random}\\ \text{movement}}}. \tag{2b}$$

Here $\mathcal{B}(t) > 0$ at times $t$ when the tidal flow is towards the shore, and $\mathcal{B}(t) < 0$ when flow is away from the shore. Mathematical modelling of tides has a history of more than two hundred years (Cartwright, 1999), and their computational study remains an active research area: Griffiths & Hill (2015) give a recent review. However such detailed work is beyond the scope of the present paper: we are looking only for a simple representation of the basic phenomenon of repeated switches in flow direction. The Wadden Sea has a semi-diurnal tide: two nearly equal high and low tides each day. We approximate this tidal pattern by taking $\mathcal{B}(.)$ to be a periodic function with zero mean. Of course tides are not actually periodic because of longer term fluctuations, but periodicity is a mathematically useful simplification that captures the essential phenomenon. To ensure uniqueness, we

impose the condition

$$\frac{1}{T}\int_{t=0}^{t=T} \left|\mathcal{B}(t)\right| dt = 1 \tag{3}$$

which ensures that the overall strength of advection depends only on the (positive) parameter $\beta$. We begin (§2) by summarising the conditions for the onset of pattern formation in (1), so that tidal flow is unidirectional. We then (§3) consider the case of piecewise constant $\mathcal{B}(.)$, meaning that $\mathcal{B}(.)$ alternates between the values of $-1$ and 1. Although not biologically realistic, this form enables detailed mathematical analysis and thus provides a valuable case study on the implications of bidirectional advection. Building on this, we then (§4) consider more general (and more realistic) forms for $\mathcal{B}(.)$. Throughout the paper we restrict attention to the onset of patterning, that is Turing (or Turing-Hopf) bifurcation points. We do not consider the wider issue of the full parameter space in which patterns occur. When all parameter values are constant, that can be studied via numerical bifurcation methods (Sherratt, 2012, 2013; Siteur *et al*, 2014). However to our knowledge this approach has never been extended to patterns in systems with temporally varying parameters; this is a natural but very challenging area for future research.

## 2 Pattern formation for unidirectional advection

Equations (1) have two homogeneous steady states: $(a, m) = (1, 0)$ and $(a_s, m_s)$ where

$$a_s = \frac{\gamma - \delta\alpha}{\delta(1-\alpha)} \qquad m_s = \frac{\alpha(\delta-\gamma)}{\gamma-\delta\alpha}\,. \tag{4}$$

We require $(a_s, m_s)$ to be positive, and stable to spatially homogeneous perturbations. Necessary and sufficient conditions for this are very complicated algebraically, but a simple sufficient condition is

$$4 > \delta > \gamma > \delta\alpha \tag{5}$$

and we assume this to hold in the remainder of the paper. An explanation for (5) is given in the Appendix; note that it is satisfied comfortably by realistic parameter estimates (van de Koppel *et al*, 2005; Wang *et al*, 2009). The onset of patterning occurs when this steady state becomes unstable to inhomogeneous perturbations. We investigate this in the standard way, by linearising (1) about $(a_s, m_s)$ and substituting the solution ansatz

$(a-a_s, m-m_s) = (\tilde{a}, \tilde{m})\exp(\lambda t + ikx)$ where $\tilde{a}$ and $\tilde{m}$ are non-zero constants. This gives a quadratic dispersion relation whose solutions have

$$\operatorname{Re}\lambda = \tfrac{1}{2}\left[-k^2 + p + s + \left\{\tfrac{1}{2}\left(\sqrt{\phi^2+\theta^2}+\phi\right)\right\}^{1/2}\right] \tag{6}$$

where

$$p = \frac{\alpha\delta(\alpha-1)}{\gamma-\delta\alpha} \qquad q = \frac{\gamma-\delta\alpha}{\delta(\alpha-1)} \tag{7a}$$

$$r = \frac{\delta\alpha(\delta-\gamma)}{\gamma-\delta\alpha} \qquad s = \frac{\alpha(\delta-\gamma)(\gamma-\delta\alpha)}{\gamma(\alpha-1)^2} \tag{7b}$$

$$\phi = \left(k^2 + p - s\right)^2 - \beta^2 k^2 + 4qr \tag{8}$$

$$\theta = -2\beta k\left(k^2 + p - s\right). \tag{9}$$

The constants $p$, $q$, $r$ and $s$ are the entries in the Jacobian matrix of the kinetics of (1) at $(a_s, m_s)$. Figure 2a shows typical plots of $\operatorname{Re}\lambda$ against $k$ as the advection parameter $\beta$ is increased. For small $\beta$, $\operatorname{Re}\lambda < 0$ for all $k$ so that the steady state is stable; but stability is lost as $\beta$ is increased and $\operatorname{Re}\lambda$ becomes positive for some values of $k$. Pattern formation is then expected, and this is confirmed in numerical simulations (Figure 2b,c). Note that the patterns move away from the shore. Intuitively this is because the model predicts higher algal densities on the off-shore side of a mussel band compared to the on-shore side, because of consumption in the band, and this causes a net growth of mussels on the off-shore side and a net loss on the on-shore side, resulting in a gradual net off-shore migration of the band. Mathematically the movement is a consequence of the unidirectional advection term and it is expected from the linear analysis because the growth rate $\lambda$ is complex-valued. However such migration is not observed in real mussel bed patterns; we will show that with a bidirectional advection term, as in (2), patterns form which do not show large scale migration.

# 3 Pattern formation for "square-tooth" advection

As a first step in the study of bidirectional advection, we consider (2) with the forcing function $\mathcal{B}$ having "square-tooth" form:

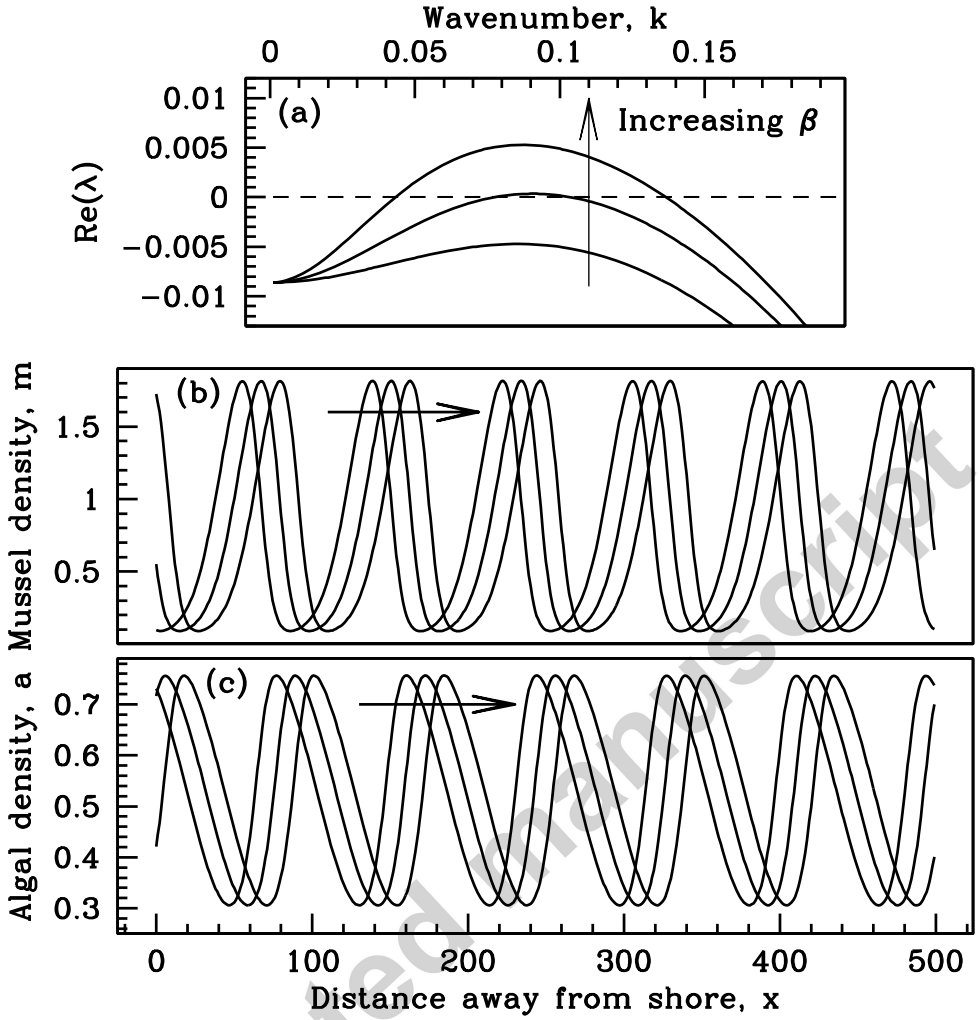


Figure 2: Pattern formation in the model (1), with unidirectional advection. (a) The dispersion relation, plotting the growth rate $\mathrm{Re}\,(\lambda)$ of small perturbations as a function of their wavenumber $k$. We show plots for $\beta = 8, 11, 15$: pattern formation occurs for values of $\beta$ greater than about 11. (b,c) A typical pattern solution. We show the mussel and algal densities $m$ and $a$ as functions of space at three equally spaced time points, to illustrate the movement of the patterns. The initial conditions for the solutions were random perturbations of the steady state $(a_s, m_s)$ and the plotted solutions are for times $t = 10\,000$, $10\,050$ and $10\,100$; the large initial time ensures that transients have dissipated. The arrows show the direction of pattern movement. The parameter values are $\alpha = 0.6667$, $\gamma = 0.1333$, $\delta = 0.15$, based on the estimates of Wang *et al* (2009). In (b) and (c) $\beta = 15$, and the equations were solved numerically using a semi-implicit finite difference scheme with upwinding.

$$\mathcal{B}(t) = \begin{cases} 1, & nT \le t < (n+\frac{1}{2})T \\ -1, & (n+\frac{1}{2})T \le t < (n+1)T \end{cases} \tag{10}$$

for any integer $n$. Such a discontinuous advection coefficient is not a realistic representation of tidal flow, but its mathematical simplicity enables detailed analysis and it is for this reason that we use it as an initial case study.

To investigate the possibility of pattern formation, we linearised (2) with (10) about $(a_s, m_s)$ and looked for solutions of the form $(a, m) = (a_s, m_s) + (\widehat{a}(t), \widehat{m}(t))e^{ikx}$, giving

$$\frac{d}{dt}\begin{bmatrix} \widehat{a} \\ \widehat{m} \end{bmatrix} = \underline{\underline{M}}^{+}\begin{bmatrix} \widehat{a} \\ \widehat{m} \end{bmatrix} \quad \text{for } nT \le t < (n+\tfrac{1}{2})T \tag{11}$$

$$\frac{d}{dt}\begin{bmatrix} \widehat{a} \\ \widehat{m} \end{bmatrix} = \underline{\underline{M}}^{-}\begin{bmatrix} \widehat{a} \\ \widehat{m} \end{bmatrix} \quad \text{for } (n+\tfrac{1}{2})T \le t < (n+1)T \tag{12}$$

$$\text{where } \underline{\underline{M}}^{\pm} = \begin{bmatrix} p \pm i\beta k & q \\ r & s - k^2 \end{bmatrix}. \tag{13}$$

For a system with periodic coefficients such as (11, 12) the stability of $(a_s, m_s)$ depends on the Floquet multipliers; an overview of Floquet theory is given in many books on ODEs, for example Jordan & Smith (2007, pp. 308-315). The piecewise constant form of (11, 12) enables the Floquet multipliers to be calculated analytically, following a methodology developed by Sherratt (1995a,b) for studying Turing pattern formation for oscillating parameters. The first step is to consider the equations in (11) and (12) separately. These equations have fundamental solutions (that is, matrices whose columns are a pair of linearly independent solutions) of the form $\underline{\underline{\Phi}}^{\pm,n}(t) = \underline{\underline{Z}}^{\pm}\underline{\underline{\Lambda}}^{\pm}(t)\underline{\underline{C}}^{\pm,n}$ where $\underline{\underline{\Lambda}}^{\pm}(t) = \mathrm{diag}[\exp(\lambda_1^{\pm}t), \exp(\lambda_2^{\pm}t)]$ with $\lambda_i^{\pm}$ being the eigenvalues of $\underline{\underline{M}}^{\pm}$ $(i = 1, 2)$, and $\underline{\underline{Z}}^{\pm}$ is a matrix whose columns are the corresponding eigenvectors. The entries of the (non-singular) matrices $\underline{\underline{C}}^{\pm,n}$ are constants of integration.

Continuity at $t = (n + 1/2)T$ gives a relation between $\underline{\underline{C}}^{+,n}$ and $\underline{\underline{C}}^{-,n}$:

$$\underline{\underline{Z}}^{-}\underline{\underline{\Lambda}}^{-}(nT + T/2)\underline{\underline{C}}^{-,n} = \underline{\underline{Z}}^{+}\underline{\underline{\Lambda}}^{+}(nT + T/2)\underline{\underline{C}}^{+,n}. \tag{14}$$

Thus there are four independent constants of integration, corresponding to arbitrary combinations of two linearly independent solutions for each column of the fundamental solution.

The Floquet multipliers are the eigenvalues of

$$\underline{\underline{\Phi}}^{+,n}(nT)^{-1}\underline{\underline{\Phi}}^{-,n}(nT + T) = \left[\underline{\underline{Z}}^{+}\underline{\underline{\Lambda}}^{+}(nT)\underline{\underline{C}}^{+,n}\right]^{-1}\underline{\underline{Z}}^{-}\underline{\underline{\Lambda}}^{-}(nT + T)\underline{\underline{C}}^{-,n}$$

$$
\begin{aligned}
&= \left[\underline{\underline{C}}^{+,n}\right]^{-1}\left[\underline{\underline{\Lambda}}^{+}(nT)\right]^{-1}\left[\underline{\underline{Z}}^{+}\right]^{-1}\underline{\underline{Z}}^{-}\,\underline{\underline{\Lambda}}^{-}(nT+T)\underline{\underline{C}}^{-,n} \\
&= \left[\underline{\underline{C}}^{+,n}\right]^{-1}\left[\underline{\underline{\Lambda}}^{+}(nT)\right]^{-1}\left[\underline{\underline{Z}}^{+}\right]^{-1}\underline{\underline{Z}}^{-}\,\underline{\underline{\Lambda}}^{-}(nT+T)\cdot \\
&\quad \left[\underline{\underline{\Lambda}}^{-}(nT+T/2)\right]^{-1}\left[\underline{\underline{Z}}^{-}\right]^{-1}\underline{\underline{Z}}^{+}\underline{\underline{\Lambda}}^{+}(nT+T/2)\underline{\underline{C}}^{+,n} \quad \text{using (14)} \\
&= \left[\underline{\underline{Z}}^{+}\underline{\underline{\Lambda}}^{+}(nT)\underline{\underline{C}}^{+,n}\right]^{-1}\underline{\underline{M}}^{-}\underline{\underline{M}}^{+}\left[\underline{\underline{Z}}^{+}\underline{\underline{\Lambda}}^{+}(nT)\underline{\underline{C}}^{+,n}\right]
\end{aligned}
$$

where $\underline{\underline{M}}^{\pm} = \underline{\underline{Z}}^{\pm}\underline{\underline{\Lambda}}^{\pm}(T/2)\left[\underline{\underline{Z}}^{\pm}\right]^{-1}$. Therefore the Floquet multipliers are the eigenvalues of $\underline{\underline{M}}^{-}\underline{\underline{M}}^{+}$.

Calculation of $\underline{\underline{M}}^{\pm}$ is straightforward, albeit algebraically laborious. It shows that the Floquet multipliers are given by $\mu = \hat{\mu}\cdot\exp(-\Gamma T/2)$, where $\hat{\mu}^2 - Y\hat{\mu} + 1 = 0$. Here

$$
\begin{aligned}
\Gamma &= k^2 - p - s && (15)\\
Y &= \tfrac{1}{2}e^{(P^+ + P^-)T/4}\left[\left(1+e^{-P^+T/2}\right)\left(1+e^{-P^-T/2}\right)\right. \\
&\quad \left. + \left(1-e^{-P^+T/2}\right)\left(1-e^{-P^-T/2}\right)\left(4qr + Q^+Q^-\right)/\left(P^+P^-\right)\right] && (16)\\
Q^{\pm} &= \pm ik\beta - k^2 - p + s && (17)\\
P^{\pm} &= \sqrt{4qr + Q^{\pm\,2}}\,. && (18)
\end{aligned}
$$

Unless either $k$ or $\beta$ is zero, $Q^{\pm}$ have non-zero imaginary parts and thus $P^{\pm}$ have non-zero real and imaginary parts; for uniqueness we take $\mathrm{Re}\,P^{\pm} > 0$. Note that $Q^{\pm}$ and hence also $P^{\pm}$ are complex conjugates, implying that $Y$ is real. Figure 3a shows a typical plot of the larger of the two values of $\log|\mu|$ against $k$ as the advection parameter $\beta$ is increased; the steady state $(a_s, m_s)$ is unstable if $|\mu| > 1$ for some value of $k$, in which case pattern formation is expected, and this is confirmed in numerical simulations (Figure 3b,c).

Comparing the results shown in Figure 3 for bidirectional advection and those in Figure 2 for unidirectional advection, the main qualitative difference concerns the movement of the patterns. In Figure 2 the pattern moves away from the shore at a constant speed, whereas in Figure 3 there is an oscillatory motion. This difference is of course entirely expected; in particular the symmetry of (2,10) in the positive and negative $x$ directions suggests that there will be no net translation of the pattern. Note that in real mussel bed patterns there is no large scale migration of the bands.

There is also a quantitative difference between the two cases: the critical value of $\beta$ at which patterns arise is slightly higher for bidirectional advection. (Note that all

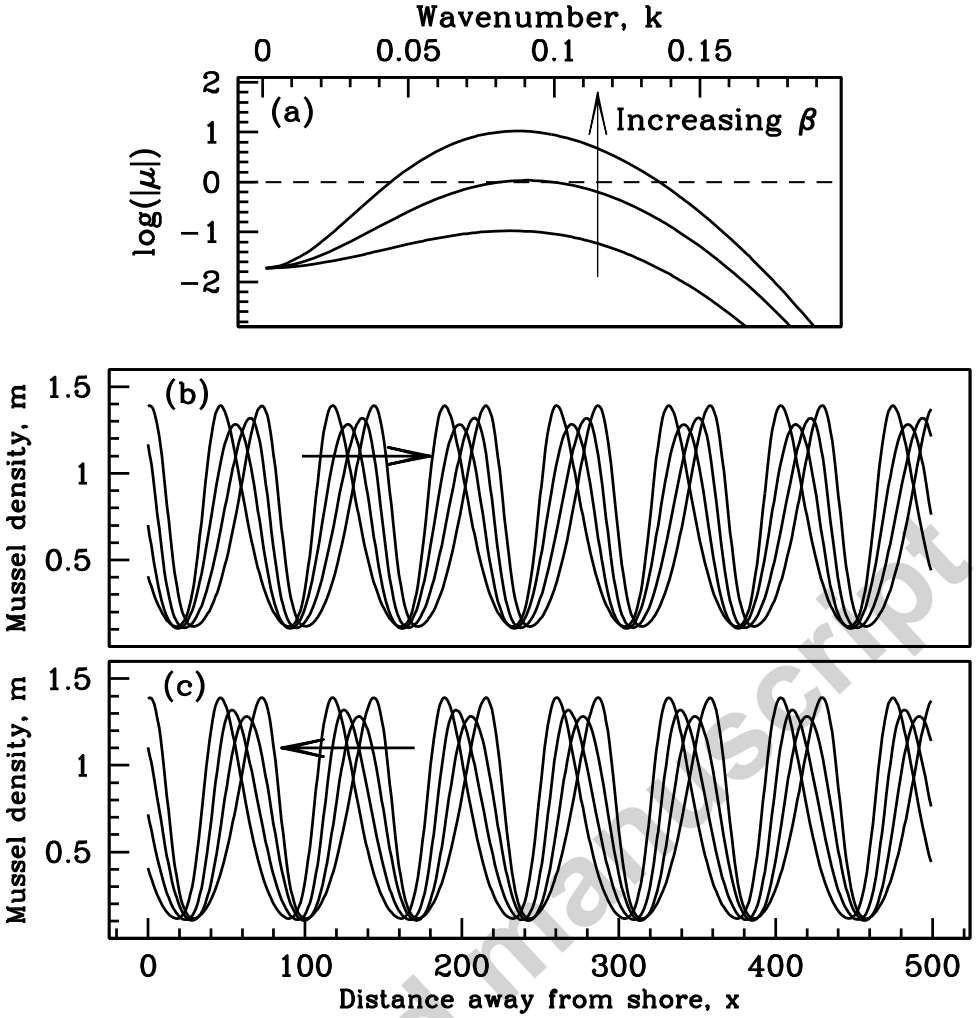


Figure 3: Pattern formation in the model (2), with bidirectional advection given by the square-tooth function (10). (a) The logarithm of the larger of the absolute values of the Floquet multipliers, plotted against wavenumber $k$. We show plots for $\beta = 8, 11, 15$: pattern formation occurs for values of $\beta$ greater than about 11. (b,c) A typical pattern solution. We show the mussel density $m$ as a function of space at seven equally spaced time points, to illustrate the movement of the patterns. The algal density $a$ has a similar solution form, except that the oscillations are partly out of phase with those for the mussel density (see Figure 2). The plots in (b) / (c) are for the halves of the forcing period in which advection is directed towards / away from the shore. The arrows show the direction of pattern movement; as expected, this is in the opposite direction to the advection. The initial conditions for the solutions were random perturbations of the steady state $(a_s, m_s)$ and the times at which the solutions are plotted are: (b) $200\,000 - T$, $200\,000 - \frac{5}{6}T$, $200\,000 - \frac{4}{6}T$, $200\,000 - \frac{3}{6}T$; (c) $200\,000 - \frac{3}{6}T$, $200\,000 - \frac{2}{6}T$, $200\,000 - \frac{1}{6}T$, $200\,000$. The large initial time ensures that transients have dissipated. The parameter values are $\alpha = 0.6667$, $\gamma = 0.1333$, $\delta = 0.15$, based on the estimates of Wang *et al* (2009); the period $T = 200$. In (b) and (c) $\beta = 15$, and the equations were solved numerically using a semi-implicit finite difference scheme with upwinding.

parameters are the same in Figures 2 and 3). This suggests that van de Koppel *et al*'s (2005) assumption of unidirectional advection leads to slight over-estimates of the propensity of the model to predict patterning. We will now investigate this in more detail by considering how the conditions for the onset of pattern formation depend on the forcing period $T$.

We begin by considering the case of large $T$. Equations (16)–(18) imply that to leading order as $T \to \infty$, $Y = \frac{1}{2} e^{P_{\rm real} T/2} \left[1 + (4qr + Q^+ Q^-)/(P^+ P^-)\right]$ where $P_{\rm real} = \mathrm{Re}\, P^\pm > 0$. Therefore $Y \to \infty$ as $T \to \infty$, and thus the two roots for $\hat{\mu} \sim Y$ and $1/Y$. The Floquet multiplier with the larger absolute value corresponds to the former root, and is

$$\mu = \tfrac{1}{2} e^{(P_{\rm real} - \Gamma)T/2} \left[1 + (4qr + Q^+ Q^-)/(P^+ P^-)\right]$$

to leading order as $T \to \infty$. Therefore the condition for $(a_s, m_s)$ to be stable is $P_{\rm real} > \Gamma = k^2 - p - s$. Comparing (17) with (8,9) shows that $Q^{\pm\,2} + 4qr = \phi \pm i\theta$. Therefore (6) can be rewritten as $\mathrm{Re}\,\lambda = \frac{1}{2}\left[-k^2 + p + s + P_{\rm real}\right]$. Hence the leading order condition for stability of $(a_s, m_s)$ in (2) as $T \to \infty$ is the same as the condition for stability in (1), the unidirectional case.

We now turn to the opposite extreme of $T \to 0$. Taylor series expansion of (16) implies

$$Y = 2 + \tfrac{1}{16}\left(P^{+\,2} + P^{-\,2} + 8qr + 2Q^+ Q^-\right) T^2 + O\left(T^3\right).$$

Therefore the Floquet multipliers are real and positive, with the larger being

$$\mu_+ = 1 + \tfrac{1}{4}\left(\sqrt{P^{+\,2} + P^{-\,2} + 8qr + 2Q^+ Q^-} - 2(k^2 - p - s)\right) T + O(T^2).$$

Now (5) implies that $p + s < 0$. Hence for small $T$ the condition $\mu_+ > 1$ for instability to a perturbation with wavenumber $k$ reduces to

$$P^{+\,2} + P^{-\,2} + 8qr + 2Q^+ Q^- > 4(k^2 - p - s)^2.$$

Substituting (17) and (18) into this inequality and simplifying shows that the condition for instability is $pk^2 > ps - qr$. Straightforward calculations show that (5) implies that $ps - qr > 0$ and $p < 0$. Therefore for sufficiently small $T$, $(a_s, m_s)$ is stable to all perturbations. Intuitively this is exactly as expected: when the advection coefficient

fluctuates rapidly between two values, one expects the behaviour to be the same as for a constant coefficient with the average of the two values, which is 0, and pattern formation cannot occur in (1) with $\beta = 0$.

These results suggest that the parameter region in which $(a_s, m_s)$ is unstable – corresponding to pattern formation – shrinks as the period $T$ decreases. To test this, we calculated the curve in the $\beta$–$\delta$ plane on which stability changes, for fixed values of the other parameters. For given values of $\beta$ and $\delta$, we used (15–18) to calculate the Floquet multipliers on a grid of $k$ values. This gives an approximation to the Floquet multiplier with largest absolute value, which we refined by fitting a parabola through the three $k$ values adjacent to the maximum. Following this procedure, we calculated the Floquet multiplier with largest absolute value on a grid of $\beta$ values, determining the critical value at which it crosses 1 by linear interpolation between grid points. Repeating this process for a succession of $\delta$ values generates the critical curves in the $\beta$–$\delta$ plane; examples are illustrated in Figure 4. As $T$ is decreased the parameter region for patterning gradually shrinks, starting at the curve for unidirectional advection in the limiting case of $T \to \infty$, and disappearing entirely as $T \to 0$.

The fact that the conditions for pattern formation depend strongly on $T$ means that we must investigate the appropriate value of $T$ for mussel beds in the Wadden Sea. The tide here changes direction about every 6.5 hours (e.g. `www.tide-forecast.com/countries/-Netherlands`), so that an appropriate value for $T$ is 13 hours; the nondimensionalisation and parameter estimates in van de Koppel *et al* (2005) imply that this corresponds to a dimensionless value of about 2000. Figure 4 shows that for this value of $T$ the difference between the region of the $\beta$–$\delta$ plane giving patterns differs only slightly from that for the unidirectional advection case: for any value of $\delta$ the critical value of $\beta$ is less than 1% lower in the bidirectional case. Thus for the parameter estimates that they use, van de Koppel *et al*'s assumption of unidirectional advection gives a very good approximation to the conditions for the onset of pattern formation – at least compared to the "square-tooth" form of bidirectional advection that we have been considering. In the next section we will show that more realistic forms for the oscillations in advection have a greater affect on the conditions for patterning.

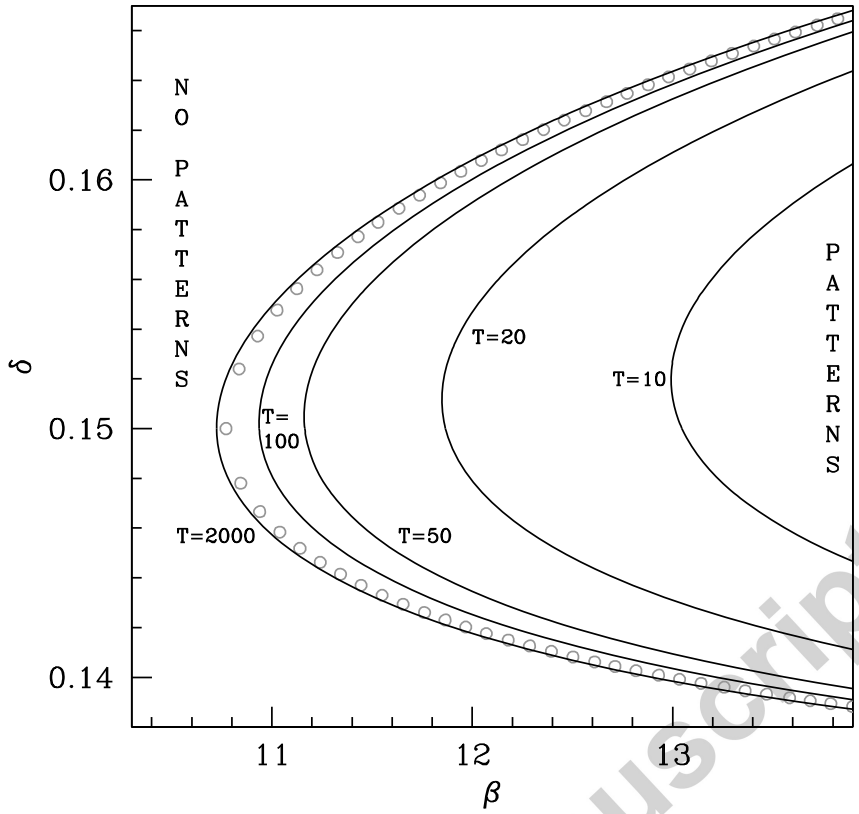


Figure 4: An illustration of the region of the $\beta$–$\delta$ parameter plane in which $(a_s, m_s)$ is unstable, giving patterns, for a sequence of values of the oscillation period $T$, when the advection rate oscillates with a square-tooth form (10). The parameter region expands with $T$, approaching the corresponding region for constant advection, which is shown by the grey circles. The other parameter values are $\alpha = 0.6667$ and $\gamma = 0.1333$, based on the estimates of Wang *et al* (2009).

# 4 Pattern formation for other forms of bidirectional advection

A major caveat to the results in the previous section is that they are restricted to the "square-tooth" functional form for the forcing function $\mathcal{B}(.)$. For general $\mathcal{B}(.)$ the Floquet multipliers cannot be calculated analytically. However numerical calculation is possible and we will use this approach to extend our analytical results for the square-tooth case to more realistic forcing functions.

Tidal flows are approximately sinusoidal. However, rather than simply use $\mathcal{B}(t) \propto \sin(2\pi t/T)$ we consider a family of forcing functions, which enables a gradual progression

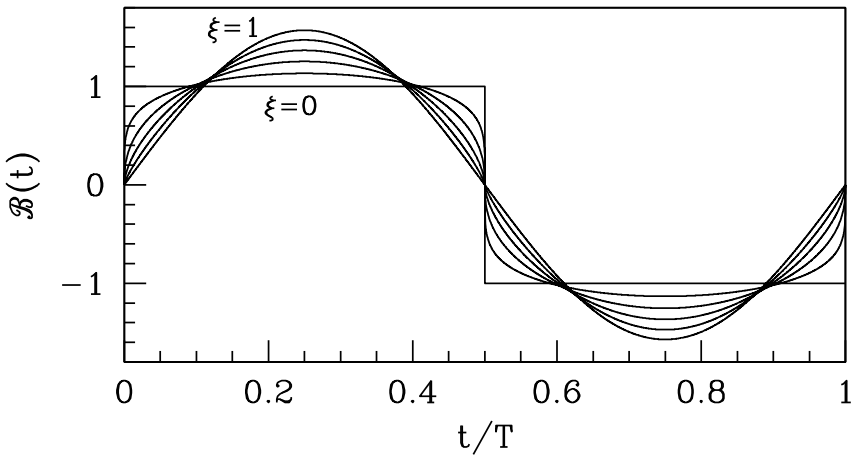


Figure 5: An illustration of the function family (19) that we use for the oscillations in algal advection. As the parameter $\xi$ increases from 0 to 1, the function gradually changes from square-tooth to sinusoidal form. The plots show the cases $\xi = 0, 0.2, 0.4, \ldots, 1$.

from the analytical results of the previous section to the more realistic sinusoidal case:

$$\mathcal{B}(t) = T \cdot \mathrm{sign}\big[\sin(2\pi t/T)\big] \cdot |\sin(2\pi t/T)|^{\xi} \Big/ \int_{\tau=0}^{\tau=T} |\sin(2\pi\tau/T)|^{\xi}\, d\tau \qquad (19)$$

(illustrated in Figure 5). Here the denominator is chosen so that (3) is satisfied. This family is parameterised by $\xi \in [0, 1]$. When $\xi = 0$ (19) gives the square-tooth form (10), while $\xi = 1$ gives a simple sinusoidal oscillation.

As in §3 we linearised (2) about $(a_s, m_s)$ and looked for solutions of the form $(a, m) = (a_s, m_s) + (\widehat{a}(t), \widehat{m}(t))e^{ikx}$. We then solved the resulting ODEs for $(\widehat{a}, \widehat{m})$ numerically over one period $T$, first using initial conditions $(\widehat{a}, \widehat{m}) = (1, 0)$ and then $(\widehat{a}, \widehat{m}) = (0, 1)$. This gives two linearly independent solutions, and we constructed a matrix with columns given by these two solutions evaluated at $t = T$. The Floquet multipliers are the eigenvalues of this matrix, which can be calculated by standard numerical linear algebra programs. We repeated this procedure over a grid of $k$ values, giving an approximation to the Floquet multiplier with largest absolute value; as in §3 we refined this using quadratic interpolation. Again as in §3, we applied this method on a grid of $\beta$ values, using linear interpolation between grid points to determine the critical value of $\beta$ at which the largest amplitude of a Floquet multiplier crosses 1. This enables calculation of the curve in the $\beta$–$\delta$ plane on which $(a_s, m_s)$ loses stability, heralding pattern formation.

Figures 6a,b show the change in this critical curve as $\xi$ is increased between 0 and 1, for

two values of the forcing period $T$. As $\xi$ increases, the parameter region giving patterns shrinks, so that for any given value $\delta$ a larger value of the advection rate $\beta$ is required for patterning. In these figures we superimpose the critical curve for unidirectional advection (grey circles). As commented previously, this curve is almost indistinguishable from that for bidirectional advection when $\xi = 0$ (square-tooth forcing) and $T$ is large. However as $\xi$ decreases the curves for the two cases separate, and further increase in $T$ does not change this: increasing $T$ above 2000 causes no visible change in the results plotted in Figure 6a. Therefore for the realistic case of sinusoidal advection ($\xi = 1$) the parameter region for patterns is significantly smaller than that given by a unidirectional advection term.

One notable aspect of the comparison between parts a and b of Figure 6 is that although there is a significant difference between the curves for $T = 2000$ and $T = 80$ when $\xi = 0$ (square-tooth forcing), there is very little difference when $\xi = 1$ (sinusoidal forcing). Further investigation revealed that for $\xi = 1$ the critical curve approaches its large $T$ limit very rapidly: for $T$ greater than about 20 there is almost no change in form (Figure 6c). Since this is two orders of magnitude lower than van de Koppel *et al*'s (2005) estimate of $T = 2000$, it follows that for the realistic case of sinusoidal advection the parameter region giving patterns is effectively independent of the period $T$.

# 5 Discussion

The model of van de Koppel *et al* (2005) for pattern formation in mussel beds assumes a constant inshore advection of algae, for reasons of mathematical simplicity. In reality, the direction of advection oscillates with the tide, and the objective of our study has been to investigate the way in which these oscillations affect the potential for pattern formation. We have shown that the assumption of unidirectional advection over-estimates the parameter region giving patterns. We considered first the case in which the advection parameter alternates between two constant values of equal magnitude but opposite sign – again in the interests of mathematical simplicity. Then the parameter region giving patterns shrinks as the period of the oscillations decreases, but when the period corresponds to the actual tidal oscillations in the Wadden Sea (about 13 hours) there is only a

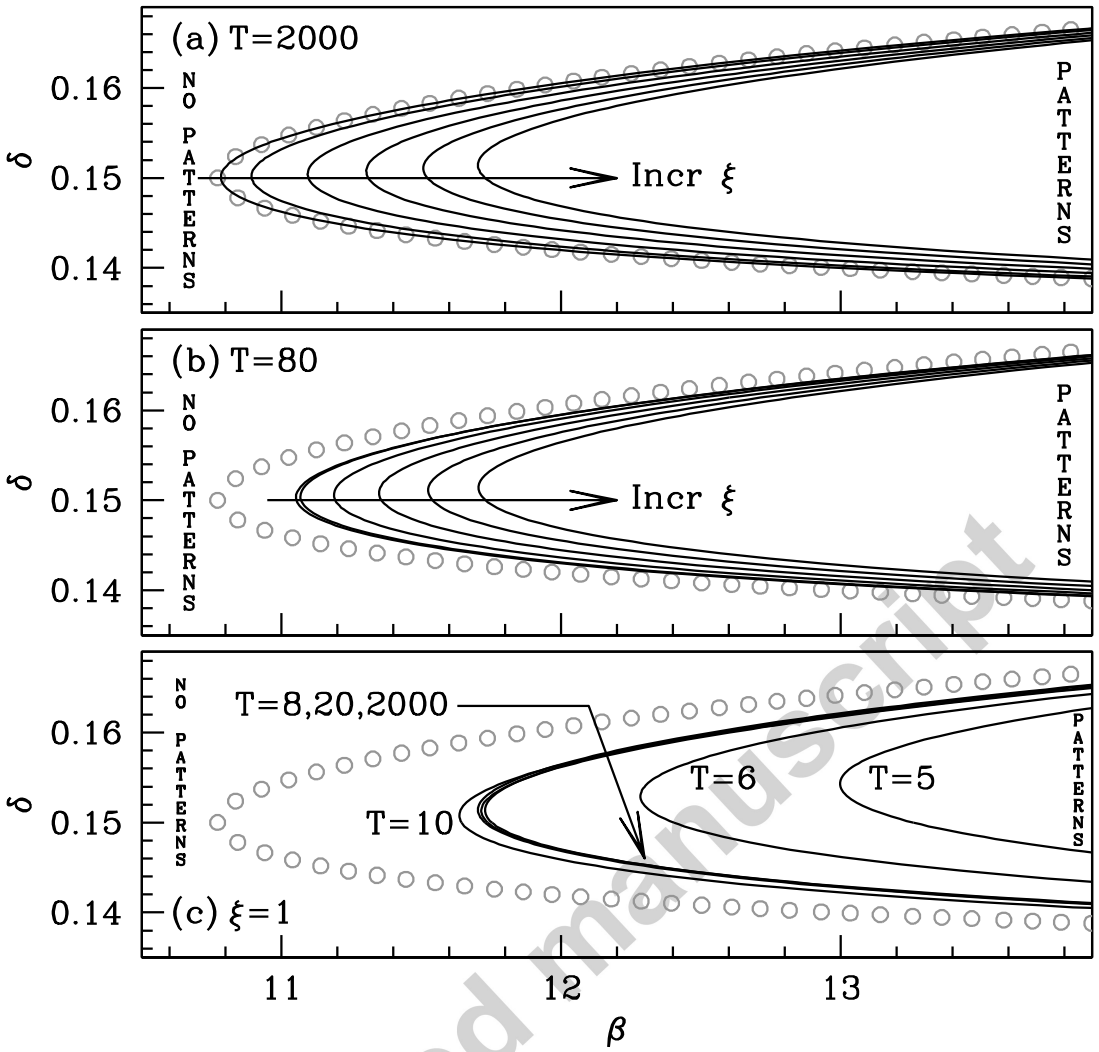


Figure 6: Illustrations of the region of the $\beta$–$\delta$ parameter plane in which $(a_s, m_s)$ is unstable, giving patterns, when the advection rate oscillates according to the function family $\mathcal{B}(t)$, defined in (19). (a,b) The region is shown for a sequence of values of the parameter $\xi$, when the period of the oscillations is (a) $T = 2000$, (b) $T = 80$. As discussed in the main text, the parameter estimates of van de Koppel *et al* (2005) imply that a dimensional period of about 2000 is appropriate for tidal flow. The parameter region giving patterns shrinks as $\xi$ increases from 0 to 1; these extreme cases correspond respectively to square-tooth and sinusoidal oscillations (see Figure 5). The grey circles indicate the parameter region giving patterns in the case of constant advection. The values of $\xi$ used are 0, 0.2, 0.4, ..., 1. (c) For $\xi = 1$ (sinusoidal oscillations) the parameter region giving patterns expands as $T$ increases, except for small oscillations for larger values of $T$. The limiting form is significantly different (smaller) than the region for constant advection, which is again shown by grey circles. Note that the parameter region is close to its limiting form even for relatively small values of $T$: the approach is much more rapid than that for square-tooth forcing (shown in Figure 4). The other parameter values are $\alpha = 0.6667$ and $\gamma = 0.1333$, based on the estimates of Wang *et al* (2009).

slight difference relative to unidirectional advection. However for the more realistic case of sinusoidal oscillations in the advection parameter, the parameter region giving patterns is significantly smaller than for unidirectional advection, even at very large periods. In addition, unidirectional advection causes a constant migration of the patterns away from the shore, which is not seen in reality, whereas oscillating advection implies small scale oscillations in the band locations, but no net migration.

There are two different reasons for the reduced propensity for pattern formation in the model with oscillatory advection, compared to the unidirectional case. The first is that the effects of advection in one direction are somewhat "cancelled out" by advection occurring in the opposite direction. This is most significant when the period of the oscillations in advection is small: indeed as the period approaches zero the advection has no effect at all. Even at very long oscillation periods there is a degree of "cancelling out", but the case of square-tooth advection considered in §3 shows that this is very slight. The second effect of oscillations in advection is that for a proportion of the time, the advection rate is quite small. This does not apply for square-tooth advection but it becomes more important as the parameter $\xi$ is increased in the forcing function family (19). For constant (unidirectional) advection, there is a critical level of the advection parameter that must be exceeded for patterns to form (van de Kopell *et al*, 2005; Wang *et al*, 2009). When the advection parameter oscillates, its absolute value is below this critical level for part of each time period. Patterns are therefore suppressed during this part of the time period, with active pattern formation being restricted to other parts of the period. This is mitigated by the fact that the absolute value of the advection parameter is larger than in the unidirectional advection case for part of each time period (see Figure 5): this is required to maintain a constant average value as specified by (3). However our results show that this mitigating effect is insufficient to prevent greater restrictions on the parameter values giving patterns, and comparison of the square-tooth and sinusoidal cases shows that this second effect of oscillatory advection is much more significant than the first.

To our knowledge, this paper is the first to investigate the effects of time-varying advection on spatial pattern formation in reaction-diffusion-advection systems. However a number of previous papers have considered patterning in reaction-diffusion systems

with time-varying diffusivity. This problem was first studied by Timm & Okubo (1992) in the context of plankton patchiness. Zooplankton often exhibit an oscillating diurnal vertical migration, spending nights near the surface and days in deeper water. The traditional explanation for this is that the ascent facilitates feeding while the descent gives greater protection from predators (e.g. Ringelberg, 2010), although alternative trade-offs have been suggested, for example between water temperature and ultraviolet radiation damage (Leach *et al*, 2015). Because horizontal ocean currents vary with depth, the oscillation in vertical migration can lead to a corresponding oscillation in horizontal dispersal. Timm & Okubo (1992) investigated the effects of this on the pattern-forming potential of zooplankton–phytoplankton systems using a predator–prey model in which the predator diffusion coefficient varied periodically in time. Using perturbation theory, they showed that a small temporal variation in dispersal rate reduces the tendency for pattern formation, and this result was extended to general predator-prey models by Gourley *et al* (1996). Both papers presented numerical simulations demonstrating a similar stabilising effect of higher amplitude oscillations in predator diffusion. However this is not a general result: analytical work by Sherratt (1995) and Bhattacharyya & Mukhopadhyay (2011) shows that oscillatory diffusion rates can promote pattern formation in some cases. These various ecology-based studies concern systems in which there are patterns of standard Turing type in the absence of time-varying diffusion. In their work on the Gray-Scott chemical reaction, Wang *et al* (2011) show that oscillatory diffusion can also induce complex spatiotemporal patterns, especially when combined with additive noise.

Mussel beds are a rich source of pattern formation problems. As well as the large-scale banded patterns considered in this paper, which have a wavelength of about 6 m, mussels also form net-shaped clusters with a length-scale of 10-20 cm (Liu *et al*, 2014b). This smaller scale patterning is thought to arise from a quite different mechanism, namely phase separation based on density-dependent movement (Liu *et al*, 2013). Many questions remain unanswered concerning both of these patterning processes and in particular about their interaction, which is predicted to increase mussel bed resilience in the model of Liu *et al* (2014b).

Understanding the dynamics of mussel beds is an important practical question. Mussel

beds are an active research system within restoration ecology; this includes work specifically on the Wadden Sea (de Paoli *et al*, 2014; van der Molen *et al*, 2015). Moreover, mussels are an economically important resource in many parts of the world: for example within the European Union the combined annual value of the mussel fishing and aquaculture industries is about 400 million euros (2009 figure)[1]. In the Wadden Sea alone, annual blue mussel landings exceeded 20 000 tons (wet weight) in every year between 1965 and 2007 (Nehls *et al*, 2009). Spatial patterning may affect both the resilience and productivity of mussel beds (Liu *et al*, 2012, 2014b) and may therefore have important implications for both restoration programs and mussel fisheries. Detailed and realistic models are required to clarify these implications. The starting point for such modelling is simple models such as that of van de Koppel *et al* (2005), which play a key role because comprehensive studies of pattern formation are possible. The next step is a gradual increase in model realism, which necessitates an increase in complexity. It is in this spirit that we have incorporated bidirectional advection into the model of van de Koppel *et al* (2005). Our prediction that this has a significant effect on the pattern forming potential of the model suggests that a more realistic representation of tidal flow will be an important component of future, more detailed models.



[1]Source: European Commission Fisheries and Aquaculture in Europe Fact Sheet No. 59, December 2012, `http://ec.europa.eu/fisheries/documentation/publications/factsheets-aquaculture--species/mussels_en.pdf`.

# Appendix

In this Appendix we discuss the conditions for the homogeneous steady state (4) to be positive and stable to spatially homogeneous perturbations. Our aim is to explain the basis for the condition (5) that we assume to be satisfied by the model parameters. Although there have been a number of previous studies of the model (1) (van de Koppel *et al*, 2005; Wang *et al*, 2009; Liu *et al*, 2012; Sherratt, 2013; Ghazaryan & Manukian, 2015; Cangelosi *et al*, 2015), none of these papers includes a detailed discussion of the stability conditions for (4).

Positive values for $a_s$ and $m_s$ requires

$$\text{either} \qquad \delta > \gamma > \delta\alpha \tag{A.1}$$

$$\text{or} \qquad \delta < \gamma < \delta\alpha\,. \tag{A.2}$$

Stability to homogeneous perturbations requires $ps > qr$ and $p + s < 0$, where $p$, $q$, $r$ and $s$ are the entries in the Jacobian matrix of the kinetics of (1) at $(a_s, m_s)$, and are given in (7). The first of these holds if (A.1) applies, but not if (A.2) applies. However (A.1) is not sufficient for stability because $p + s$ may have either sign.

Using (7), $p + s < 0$ if and only if

$$\gamma\delta(1-\alpha)^3 > (\delta-\gamma)(\gamma-\delta\alpha)^2\,.$$

We rewrite this inequality as $\mathcal{G}_1(\sigma) > \mathcal{G}_2(\sigma)$ where $\sigma = \gamma/\delta$, and

$$\mathcal{G}_1 = \sigma/\delta \text{ and } \mathcal{G}_2 = (1-\sigma)(\sigma-\alpha)^2/(1-\alpha)^3\,. \tag{A.3}$$

There is a (unique) critical value $\delta_{\rm crit}(\alpha)$ at which the linear function $\mathcal{G}_1(\sigma)$ touches the cubic $\mathcal{G}_2(\sigma)$. The two insets in Figure A.1a show example plots of $\mathcal{G}_1$ and $\mathcal{G}_2$ when $\delta$ is above and below $\delta_{\rm crit}$. The algebraic form of $\delta_{\rm crit}$ is very complicated but numerical calculation is straightforward, and its variation with $\alpha$ is shown in Figure A.1a. When $\delta < \delta_{\rm crit}(\alpha)$, $\mathcal{G}_1$ will be greater than $\mathcal{G}_2$ for all $\alpha$ and $\gamma$ satisfying (A.1).

Figure A.1a suggests that $\delta_{\rm crit}$ is an increasing function of $\alpha$. To prove this, we first note that (A.1) corresponds to $\sigma \in (\alpha, 1)$. On this interval, $\mathcal{G}_2(\sigma)$ has a unique local

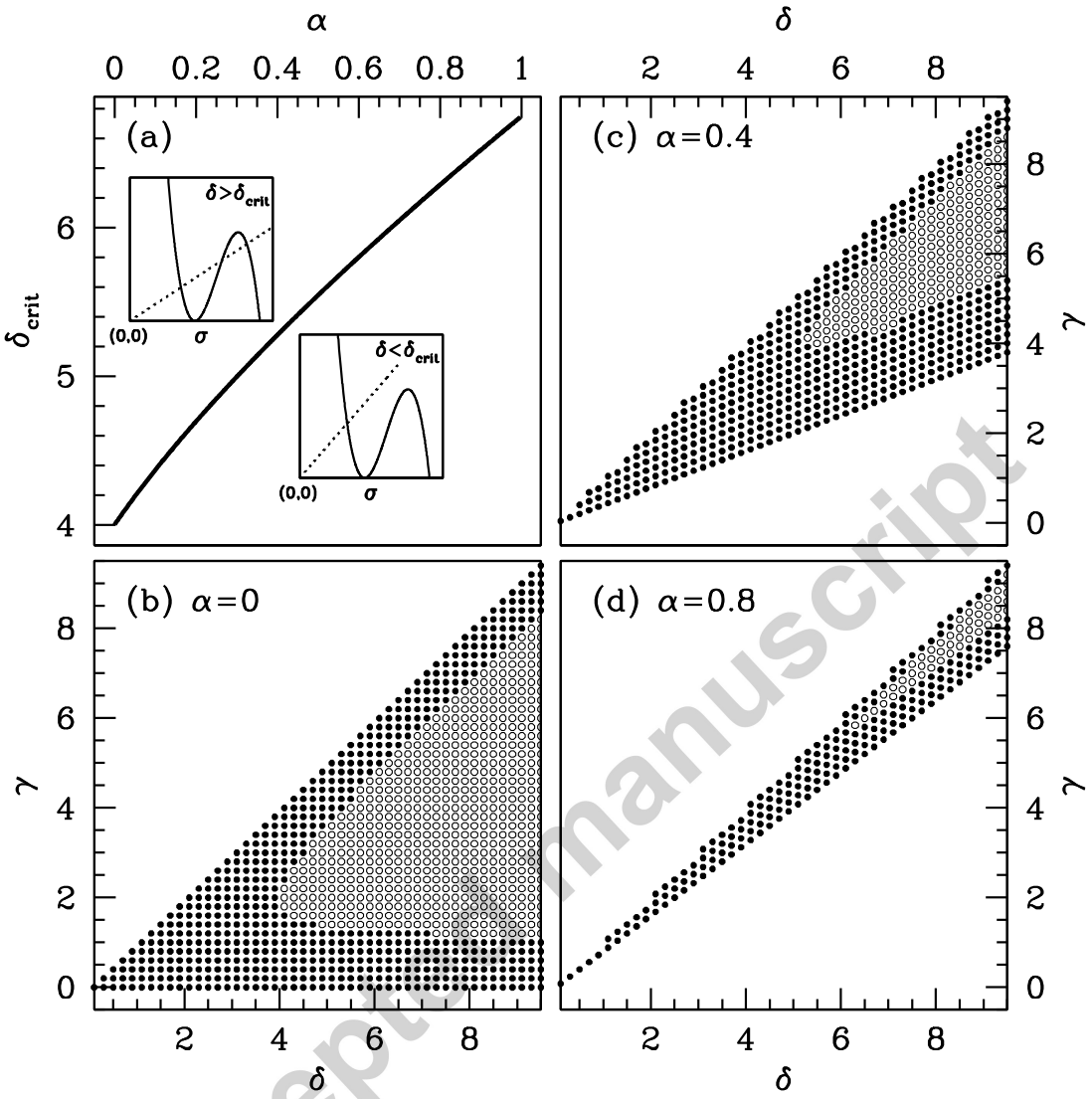


Figure A.1: (a) A plot of $\delta_{\text{crit}}$ against $\alpha$; as explained in the main text of the Appendix, $\delta = \delta_{\text{crit}}$ is the condition for $\mathcal{G}_1(\sigma)$ and $\mathcal{G}_2(\sigma)$ to touch. The two insets show example plots of $\mathcal{G}_1(\sigma)$ (dashed line) and $\mathcal{G}_2(\sigma)$ (solid line) against $\sigma$, for $\delta$ either side of $\delta_{\text{crit}}$. The insets both use $\alpha = \frac{1}{2}$, with $\delta = 7$ (upper left inset) and $\delta = 4$ (lower right inset). For both insets the axes ranges are $[0, 1.1]$ on the horizontal axis, and $[0, 0.03]$ on the vertical axis. (b-d) Parameter planes showing the regions in which $(a_s, m_s)$ is stable ($\bullet$) and unstable ($\circ$); unmarked regions are those not satisfying (A.1). Therefore the regions marked with filled circles ($\bullet$) are those in which $(a_s, m_s)$ is positive and stable to spatially homogeneous perturbations. Note that for all values of $\alpha$, the open circles ($\circ$) all lie to the right of $\delta = 4$.

maximum, at $\sigma = (2+\alpha)/3$. Therefore the value $\sigma$ at which $\mathcal{G}_1$ and $\mathcal{G}_2$ touch when $\delta = \delta_{\text{crit}}$ must lie between $\alpha$ and $(2+\alpha)/3$. But

$$d\mathcal{G}_2/d\alpha = (3\sigma - \alpha - 2)(1-\sigma)(\sigma-\alpha)\big/(1-\alpha)^4$$

which is $< 0$ for $\sigma \in \big(\alpha, (2+\alpha)/3\big)$. Therefore the slope of the linear function $\mathcal{G}_1$ at which it touches $\mathcal{G}_2$ must decrease as $\alpha$ increases, i.e. $d\delta_{\text{crit}}/d\alpha > 0$. It follows that for all $\alpha$ satisfying (A.1), $\delta_{\text{crit}}(\alpha) > \delta_{\text{crit}}(0)$. But when $\alpha = 0$, $\mathcal{G}_2 = \sigma^2(1-\sigma)$ implying that $\delta_{\text{crit}}(0) = 4$. Therefore if $\delta < 4$ and (A.1) both hold, then $(a_s, m_s)$ is positive and also stable to spatially homogeneous perturbations.

As a final comment we emphasise that $(a_s, m_s)$ may be stable when $\delta > 4$, but that this requires additional restrictions on $\alpha$ and $\gamma$, beyond (A.1). Figure 4b–d shows $\delta$–$\gamma$ parameter planes for three values of $\alpha$, with the regions of stability and instability indicated by solid and open circles respectively; regions not marked by circles are those in which (A.1) is not satisfied. At the interface between the closed and open circles, the kinetics of (1) undergo a Hopf bifurcation, implying temporal oscillations that are not observed in real mussel beds – this is consistent with the fact that realistic parameter estimates comfortably satisfy (5) (van de Koppel *et al*, 2005; Wang *et al*, 2009).

# References

Bekker, M.F., Clark, J.T., Jackson, M.W. 2009. Landscape metrics indicate differences in patterns and dominant controls of ribbon forests in the Rocky Mountains, USA. Appl. Veg. Sci. 12, 237-249.

Bertness, M.D., Grosholz, E. 1985. Population dynamics of the ribbed mussel, *Geukensia demissa*: the costs and benefits of an aggregated distribution. Oecologia 67, 192-204.

Bhattacharyya, R., Mukhopadhyay, B. 2011. On a population pathogen model incorporating species dispersal with temporal variation in dispersal rate. J. Biol. Phys. 37, 401-416.

Cangelosi, R.A., Wollkind, D.J., Kealy-Dichone, B.J., Chaiya, I. 2014. Nonlinear stability analyses of Turing patterns for a mussel-algae model. J. Math. Biol. 70, 1249-1294.

Cartwright, D.E. 1999. Tides: A Scientific History. Cambridge University Press, Cambridge, UK.

Commito, J.A., Commito, A.E., Platt, R.V., Grupe, B.M., Piniak, W.E., Gownaris, N.J., Reeves, K.A., Vissichelli, A.M. 2014. Recruitment facilitation and spatial pattern formation in soft-bottom mussel beds. Ecosphere 5(12), 160.

Côté, I.M., Jelnikar, E. 1999. Predator-induced clumping behaviour in mussels (*Mytilus edulis Linnaeus*). J. Exp. Mar. Biol. Ecol. 235, 201-211.

de Paoli, H., van de Koppel, J., van der Zee, E., Kangeri, A., van Belzen, J., Holthuijsen, S., van den Berg, A., Herman, P., Olff, H., van der Heide, T. 2015. Processes limiting mussel bed restoration in the Wadden-Sea. J. Sea Res. 103, 42-49.

Deblauwe, V., Barbier, N., Couteron, P., Lejeune, O., Bogaert, J. 2008. The global biogeography of semi-arid periodic vegetation patterns. Global Ecol. Biogoegr. 17, 715-723.

Deblauwe, V., Couteron, P., Lejeune, O., Bogaert, J., Barbier, N. 2011. Environmental modulation of self-organized periodic vegetation patterns in Sudan. Ecography 34, 990-1001.

455 Dolmer, P. 2000. Algal concentration profiles above mussel beds. J. Sea Res. 43, 113-119.

456 Donker, J. 2015. Hydrodynamic processes and the stability of intertidal mussel beds in
457 the Dutch Wadden Sea. PhD thesis, Utrecht University, Netherlands.

458 Donker, J.J., van der Vegt, M., Hoekstra, P. 2015. Erosion of an intertidal mussel bed by
459 ice- and wave-action. Cont. Shelf Res. 106, 60-69.

460 Eppinga, M.B., Rietkerk, M., Borren, W., Lapshina, E.D., Bleuten, W., Wassen, M.J.
461 2008. Regular surface patterning of peatlands: confronting theory with field data. Ecosys-
462 tems 11, 520-536.

463 Eppinga, M.B., Rietkerk, M., Wassen, M.J., De Ruiter, P.C. 2009. Linking habitat
464 modification to catastrophic shifts and vegetation patterns in bogs. Plant Ecol. 200,
465 53-68.

466 Ghazaryan, A., Manukian, V. 2015. Coherent structures in a population model for mussel-
467 algae interaction. SIAM J. Appl. Dyn. Syst. 14, 893-913.

468 Gourley, S.A., Britton, N.F., Chaplain, M.A.J., Byrne, H.M. 1996. Mechanisms for sta-
469 bilisation and destabilisation of systems of reaction-diffusion equations. J. Math. Biol.
470 34, 857-877.

471 Griffiths, S.D., Hill, D.F. 2015. Tidal modeling. In: Shennan, I., Long, A.J., Horton,
472 B.P., Handbook of Sea-Level Research, Wiley, Chichester, UK, pp. 438-451.

473 Jordan, D.W., Smith P. 2007. Nonlinear Ordinary Differential Equations: An Introduc-
474 tion for Scientists and Engineers. Oxford University Press, Oxford, UK.

475 wa Kangeri, A.K., Jansen, J.M., Barkman, B.R., Donker, J.J., Joppe, D.J., Dankers,
476 N.M. 2014. Perturbation induced changes in substrate use by the blue mussel, *Mytilus*
477 *edulis*, in sedimentary systems. J. Sea Res. 85: 233-240.

478 Leach, T.H., Williamson, C.E., Theodore, N., Fischer, J.M., Olson, M.H. 2015. The role
479 of ultraviolet radiation in the diel vertical migration of zooplankton: an experimental test
480 of the transparency-regulator hypothesis. J. Plankton Res. 37, 886-896.

Levin, S.A., Paine, R.T. 1974. Disturbance, patch formation, and community structure. Proc. Natl. Acad. Sci. USA 71, 2744-2747.

Liu, Q.-X., Weerman, E.J., Herman, P.M., Olff, H., van de Koppel, J. 2012. Alternative mechanisms alter the emergent properties of self-organization in mussel beds. Proc. R. Soc. Lond. B 14, 20120157.

Liu ,Q.-X., Doelman, A., Rottschäfer, V., de Jager, M., Herman, P.M., Rietkerk M., van de Koppel, J. 2013. Phase separation explains a new class of self-organized spatial patterns in ecological systems. Proc. Natl. Acad. Sci. USA 110, 11905-11910.

Liu, Q.-X., Weerman, E.J., Gupta, R., Herman, P.M., Olff, H., van de Koppel, J. 2014a. Biogenic gradients in algal density affect the emergent properties of spatially self-organized mussel beds. J. R. Soc. Interface 11, 20140089.

Liu, Q.-X., Herman, P.M., Mooij, W.M., Huisman, J., Scheffer, M., Olff, H., van de Koppel, J. 2014b. Pattern formation at multiple spatial scales drives the resilience of mussel bed ecosystems. Nat. Commun. 5, 5234.

Meron, E. 2012. Pattern-formation approach to modelling spatially extended ecosystems. Ecol. Modelling 234, 70-82.

Nehls, G., Witte, S., Dankers, N., de Vlas, F., Kristensen, P.S. 2009. Wadden Sea Ecosystem No. 25: Quality Status Report 2009, Thematic Report No. 3.3: Fisheries. Common Wadden Sea Secretariat Trilateral Monitoring and Assessment Group, Wilhelmshaven, Germany. (`http://www.waddensea-secretariat.org/sites/default/files/downloads/03.3-fishery-10-03-14-rev.pdf`)

Nicastro, K.R., Zardi, G.I., McQuaid, C.D. 2008. Movement behaviour and mortality in invasive and indigenous mussels: resilience and resistance strategies at different spatial scales. Mar. Ecol. Prog. Ser. 372, 119-126.

Øie, G., Reitan, K.I., Vadstein, O., Reinertsen, H. 2002. Effect of nutrient supply on growth of blue mussels (*Mytilus edulis*) in a landlocked bay. In: Vadstein, O., Olsen, Y. (eds.) Sustainable Increase of Marine Harvesting: Fundamental Mechanisms and New

508 Concepts, Kluwer Academic Publishers, Dordrecht, Netherlands, pp. 99-109.

509 Paine, R.T., Levin, S.A. 1981. Intertidal landscapes: disturbance and the dynamics of
510 pattern. Ecol. Monogr. 51, 145-178.

511 Pelletier, J.D., DeLong, S.B., Orem, C.A., Becerra, P., Compton, K., Gressett, K., Lyons-
512 Baral, J., McGuire, L.A., Molaro, J.L., Spinler, J.C. 2012. How do vegetation bands form
513 in dry lands? Insights from numerical modeling and field studies in southern Nevada,
514 USA. J. Geophys. Res. 117, F04026.

515 Naddafi, R., Pettersson, K., Eklöv, P. 2010. Predation and physical environment structure
516 the density and population size structure of zebra mussels. J. N. Am. Benthol. Soc. 29,
517 444-453.

518 Ringelberg, J. 2010. Diel Vertical Migration of Zooplankton in Lakes and Oceans. Springer,
519 New York.

520 Sheffer, E., Hardenberg, J., Yizhaq, H., Shachak, M., Meron, E. 2013. Emerged or
521 imposed: a theory on the role of physical templates and self-organisation for vegetation
522 patchiness. Ecol. Lett. 16, 127-139.

523 Sherratt, J.A. 1995a. Turing bifurcations with a temporally varying diffusion coefficient.
524 J. Math. Biol. 33, 295-308.

525 Sherratt, J.A. 1995b. Diffusion driven instability in oscillating environments. Eur. J.
526 Appl. Math. 6, 355-372.

527 Sherratt, J.A. 2012. Numerical continuation methods for studying periodic travelling
528 wave (wavetrain) solutions of partial differential equations. Appl. Math. Computation
529 218, 4684-4694.

530 Sherratt, J.A. 2013. History-dependent patterns of whole ecosystems. Ecol. Complex. 14,
531 8-20.

532 Sherratt, J.A. 2015. Using wavelength and slope to infer the historical origin of semi-arid
533 vegetation bands. Proc. Natl. Acad. Sci. USA 112, 4202-4207.

534 Siteur, K., Siero, E., Eppinga, M.B., Rademacher, J., Doelman, A., Rietkerk, M. 2014.
535 Beyond Turing: the response of patterned ecosystems to environmental change. Ecol.
536 Complex. 20, 81-96.

537 Snover, M.L., Commito, J.A. 1998. The fractal geometry of *Mytilus edulis L.* spatial
538 distribution in a soft-bottom system. J. Exp. Mar. Biol. Ecol. 223, 53-64.

539 Stewart, J., Parsons, A.J., Wainwright, J., Okin, G.S., Bestelmeyer, B., Fredrickson, E.L.,
540 Schlesinger, W.H. 2014. Modelling emergent patterns of dynamic desert ecosystems. Ecol.
541 Monogr. 84, 373-410.

542 Suzuki, S.N., Kachi, N., Suzuki, J.-I. 2012. Variability of local spatial structure in a
543 wave-regenerated *Abies* forest. Ecol. Res. 27, 893-901.

544 Tam, J.C., Scrosati, R.A. 2014. Distribution of cryptic mussel species (*Mytilus edulis* and
545 *M. trossulus*) along wave exposure gradients on northwest Atlantic rocky shores. Mar.
546 Biol. Res. 10, 51-60.

547 Timm, U., Okubo, A. 1992. Diffusion-driven instability in a predator-prey system with
548 time-varying diffusivities. J. Math. Biol. 30, 307-320.

549 Toomey, M.B., McCabe, D., Marsden, J.E. 2002. Factors affecting the movement of adult
550 zebra mussels (*Dreissena polymorpha*). J. N. Am. Benthol. Soc. 21, 468-475.

551 van der Molen, F., Puente-Rodrguez, D., Swart, J.A., van der Windt, H.J. 2015. The
552 coproduction of knowledge and policy in coastal governance: integrating mussel fisheries
553 and nature restoration. Ocean Coast. Manage. 106, 49-60.

554 van de Koppel, J., Rietkerk, M., Dankers, N., Herman, P.M. 2005. Scale-dependent
555 feedback and regular spatial patterns in young mussel beds. Am. Nat. 165, E66-77.

556 van de Koppel, J., Gascoigne, J.C., Theraulaz, G., Rietkerk, M., Mooij, W.M., Herman,
557 P.M. 2008. Experimental evidence for spatial self-organization and its emergent effects in
558 mussel bed ecosystems. Science 322, 739-742.

559 Wang, R.H., Liu, Q.-X., Sun, G.Q., Jin, Z., van de Koppel, J. 2009. Nonlinear dynamic
560 and pattern bifurcations in a model for spatial patterns in young mussel beds. J. R. Soc.

561 Interface 6, 705-718.

562 Wang, W., Lin, Y., Yang, F., Zhang, L., Tan, Y. 2011. Numerical study of pattern
563 formation in an extended Gray-Scott model. Commun. Nonlinear Sci. Numer. Simul. 16,
564 2016-2026.

565 Wootton, J.T. 2001. Local interactions predict large-scale pattern in empirically derived
566 cellular automata. Nature 413, 841-844.

567 Zelnik, Y.R., Meron, E., Bel, G. 2015. Gradual regime shifts in fairy circles. Proc. Natl.
568 Acad. Sci. USA 112, 12327-12331.